Visual Neuroscience (1998), **15**, 425–438. Printed in the USA.

The intrinsic dynamics of retinal bipolar cells isolated from tiger salamander

BU-QING MAO,[1,*] PETER R. MACLEISH,[2,**] AND JONATHAN D. VICTOR[1]

[1]Departments of Neurology and Neuroscience, Cornell University Medical College, New York
[2]Department of Ophthalmology, Dyson Vision Research Institute, Cornell University Medical College, New York

(RECEIVED: July 11, 1997; ACCEPTED October 23, 1997)

Abstract

We studied how intrinsic membrane properties affect the gain and temporal pattern of response in bipolar cells dissociated from retinae of tiger salamanders. Currents specified by a pseudorandom binary sequence, an m-sequence, superimposed on various means, were injected into the cells. From the resultant membrane voltage response for each mean current, impulse responses were estimated. From each impulse response, transfer function, gain, and time constant were calculated. The bipolar cells acted as quasilinear adaptive filters whose gain and response speed are determined by the mean input current. Near resting potential, gain, and time constant were maximum. Dynamics were slow and low-pass, characterized by an approximately exponential impulse response. With depolarization, gains were reduced sharply, responses were much faster, and dynamics became band-pass, as indicated by an undershoot in the impulse response. For any given mean current, the shape of the impulse response did not depend on the amplitude of the m-sequence currents. Thus, bipolar cells behaved in a quasilinear fashion. The adaptive behavior was eliminated by blocking a potassium current, which implicates the role of a voltage-gated potassium conductance. Computer simulations on a model neuron including a delayed-rectifier reconstructed the observed behavior, and provided insight into other, less readily observable, parameters. Thus, bipolar cells, even when isolated, possess mechanisms which regulate, with unsuspected elaborateness, the sensitivities and dynamics of their responsiveness. Implications for adaptation and neuronal processing are discussed.

Keywords: Current-clamp, m-sequence, Impulse response, Potassium channel, Adaptive filter

Introduction

Bipolar cells receive the first synaptic inputs in the retina. Yet many of the receptive-field characteristics of neurons later in visual pathway are already seen in bipolar cells, including antagonistic center-surround organization and double color opponency (Kaneko & Tachibana, 1981). Bipolar cells also initiate the separation of visual information into parallel streams, ON and OFF, for later stages of information processing (Shiells et al., 1981; Slaughter & Miller, 1981). A thorough understanding of the bipolar cell thus contributes to understanding the strategies by which information is encoded and processed in the retina and in the nervous system at large.

Although most studies of bipolar or other retinal neurons have been directed towards understanding their spatial properties, temporal properties are equally important. Bipolar cells are a part of a synapse in which extremely high synaptic gain can be achieved (Ashmore & Falk, 1979, 1980) and in which gain is modulated by adaptation states (Wu, 1991; Wu & Yang, 1992). The transfer properties of the synapses formed with different types of bipolar cells show different temporal properties (Ashmore & Copenhagen, 1980), and there are also differences between the receptor-bipolar synapse and the receptor-horizontal synapse (Copenhagen et al., 1983; Belgum & Copenhagen, 1988). A multistage, lead-lag filter was needed to fit the measured transfer functions of receptor-bipolar or receptor-horizontal synapses. However, the physiological basis of the lead stages, as well as the low-pass stages, remains uncertain. Moreover, a direct assessment of the bipolar cells' intrinsic transfer properties is not yet available.

The temporal resolution of vision sets the time window in which visual information is integrated (see Hart, 1987). A major determinant of temporal response properties is the adaptation state of the retina (Kelly, 1972; Enroth-Cugell & Shapley, 1973; Baylor & Hodgkin, 1974; Ashmore & Falk, 1980). Light adaptation reduces gain and increases response speed of retinal cells (Tranchina et al., 1984; Purpura et al., 1990). Adaptation begins in photoreceptors (Nakatani & Yau, 1988), but its mechanism is not entirely understood and must also be postreceptoral at least in part (Purpura et al., 1990). The changes in gain and dynamics we studied here in isolated bipolar cells bear fascinating similarities to

Reprint requests to: Bu-Qing Mao, Department of Neurobiology, University of Alabama School of Medicine, 1719 Sixth Avenue South—CIRC 425, Birmingham, AL 35294-0021, USA.

*Department of Neurobiology, University of Alabama School of Medicine, 1719 6th Avenue South, Birmingham, AL 35294, USA.

**Neuroscience Institute, Morehouse School of Medicine, 720 Westview Drive, S.W. Atlanta, GA 30310, USA.

those observed in other retinal cells (Tranchina et al., 1984; Purpura et al., 1990), and raise the possibility that these adaptive changes may share a common mechanism.

Membrane properties of bipolar cells have been studied both in isolated cells (Lasater et al., 1984; Kaneko & Tachibana, 1985; Tessier-Lavigne et al., 1988; Lasater, 1988; Karschin & Wässle, 1990) and in retinal slices (Tessier-Lavigne et al., 1988; Lasansky, 1992; Tian & Slaughter, 1995). Questions remain as to whether, and precisely how, voltage-dependent ion channels shape visual responses, even though the general importance of voltage-dependent channels in the retinal signal processing has been recognized (Attwell, 1986; Kaneko & Tachibana, 1986).

In this study, we examined the gain and temporal features of isolated bipolar cells' responses and how they are shaped by membrane conductances. We adopted a pseudorandom binary sequence, an m-sequence (Sutter, 1987; Victor, 1992), as current inputs to bipolar cells isolated from tiger salamanders (MacLeish et al., 1983). The dynamics of the bipolar cell transfer properties can be described as adaptive: depolarization from the resting potential induces a tradeoff between the gain and speed of response, and a transition between slow, low-pass behavior and faster, band-pass behavior (Mao et al., 1995). The ionic channel mechanisms underlying these changes were demonstrated by various blocking agents and further studied by computer simulations (Mao et al., 1996).

Methods

Cell dissociation and recording

Retinae of tiger salamanders (*Ambystoma tigrinum*; from Kons Scientific Co., Inc., Germantown, WI) were dissociated (MacLeish et al., 1984). The enzymatic solution contained 10 units/ml papain (Worthington Biochemical Corp., Freehold, NJ), and (in mM): 84 NaCl, 3 KCl, 25 $NaHCO_2$, 0.5 NaH_2PO_4, 1 Na pyruvate, 0.5 $CaCl_2$, 16 glucose, 2 d,l-cysteine HCl, 0.02 phenol red, and was bubbled with 5% CO_2 and 95% O_2. The retinae were digested for 30–45 min, triturated, and the isolated cells plated onto coverslips pretreated with the antibody Sal-1 (MacLeish et al., 1983). Culture medium contained (in mM): 108 NaCl, 3 KCl, 0.5 $MgCl_2$, 0.5 $MgSO_4$, 1 $NaHCO_3$, 0.5 NaH_2PO_4, 1 Na pyruvate, 0.1 choline Cl, 1.8 $CaCl_2$, 1 HEPES, 16 glucose, 0.02 phenol red, and bovine serum albumin, 50 μg/ml. pH was adjusted to 7.2 to 7.4, and osmolarity to 240 mosM.

Whole-cell patch-clamp recordings were made at room temperature (*ca.* 23°C) and typically within 2 days after dissociation. Composition of recording medium is (in mM): 108 NaCl, 3 KCl, 2.5 $CaCl_2$, 1 $MgCl_2$, 16 glucose, 5 HEPES, and 0.02 phenol red, with pH adjusted to 7.2–7.4 and osmolarity to 240 mosM. An EPC-7 amplifier, interfaced to a 486 PC *via* a DMA interface TL-1, was used for recording. PCLAMP6 software (Axon Instruments, Inc., Foster City, CA) was used for data acquisition and for the analysis of responses to conventional voltage or current steps. Electrodes were made from borosilicate micropipettes (Drummond Scientific Company, Broomall, PA) on a BB-CH-PC puller (Mecanex S.A., Switzerland), and had a tip opening of 1 μm and a resistance of 5–15 MΩ when filled with a pipette solution which contained (in mM): 113 KCl, 0.05 EGTA, 1 ATP, 5 $MgCl_2$, and 10 HEPES (with pH adjusted to 7.2 and osmolarity to 240 mosM). For certain purposes, modified pipette solutions were used, and will be specified where appropriate. Photomicrographs were taken of cells for estimating specific capacitance.

M-sequence currents to study dynamics

To characterize the dynamics of isolated cells, we injected fluctuating currents whose means are varied and whose temporal profiles are determined by a binary sequence (with values 1 and -1): the maximum-length shift-register sequence, or m-sequence. For details about the applications of the sequence to systems analysis, refer to Sutter (1987) and Victor (1992). An m-sequence, m_i, of order M, has a length of $N = 2^M - 1$ (we used $M = 11$ and $N = 2047$). The dimensionless sequence was translated into the actual currents, $S(t)$, as follows:

$$S(t) = \mu + \alpha m_i, \qquad \text{for } iT_s \le t < (i+1)T_s \tag{1}$$

in which α (in pA) is the current scale factor, T_s (in μs) is the time interval, and μ (in pA) is the mean current. The mean current μ determines if the cell will be depolarized (if $\mu > 0$), hyperpolarized (if $\mu < 0$), or kept at resting potential (if $\mu = 0$).

Fig. 1 illustrates an m-sequence current $S(t)$ (with $\mu = 100$ pA, $\alpha = 98$ pA, and $T_s = 150$ μs) and a bipolar cell's membrane voltage responses. The voltage responses can be viewed as containing two components: a steady-state component (represented by the mean of the membrane voltage) and a dynamic component (reflected in the fluctuations in the membrane voltage). From the dynamic component, we estimated the impulse response, $h(t)$, which is a concise and complete characterization of a system to the extent that it is linear. $h(t)$ can be estimated by a crosscorrelation between the voltage response and the m-sequence current, provided that the impulse response declines to zero prior to the end of an m-sequence cycle ($2^M - 1$) and that the time interval T_s between consecutive m-sequence samples is sufficiently brief. The relationship among the discretized impulse response, $h_n = h(nT_s)$, the m-sequence current, $S_n = S(nT_s)$, and the response to the m-sequence, $r_n = r(nT_s)$, is (Mao, 1996):

$$\frac{1}{\alpha^2 \cdot T_s} \langle r_n \cdot S_{n-k} \rangle = \frac{N+1}{N} \cdot h_k - \frac{1}{N} \cdot \sum_{i=0}^{N-1} h_i \tag{2}$$

For a real biological system, which is not rigorously linear, the m-sequence approach estimates the "first-order Wiener kernel," which in some sense is the best approximation to an impulse response (Marmarelis & Marmarelis, 1978). We used the method of inverse repeats (Sutter, 1987) to improve this approximation by removing contributions from even-order nonlinearities.

The robustness of the m-sequence method was assessed in numerical tests of a model neuron which contained an *RC* circuit (R and C in parallel) and a series resistance R_s. Current considered as input and voltage as output, the model neuron has an impulse response of

$$h(t) = R_s \cdot \delta(t) + \frac{1}{C} \cdot e^{-t/RC} \tag{3}$$

The effect of the series resistance R_s is reflected in the term $R_s \cdot \delta(t)$ in eqn. (3), and is concentrated at $t = 0$. In the numerical tests, it was contained only in the first data point $h_0 = 1/C + R_s/T_s$. With this information, parameters C, R, and R_s were estimated from the impulse responses and found to be in good agreement with their known values (Mao, 1996). However, in impulse responses estimated from actual recordings, the effect of any series

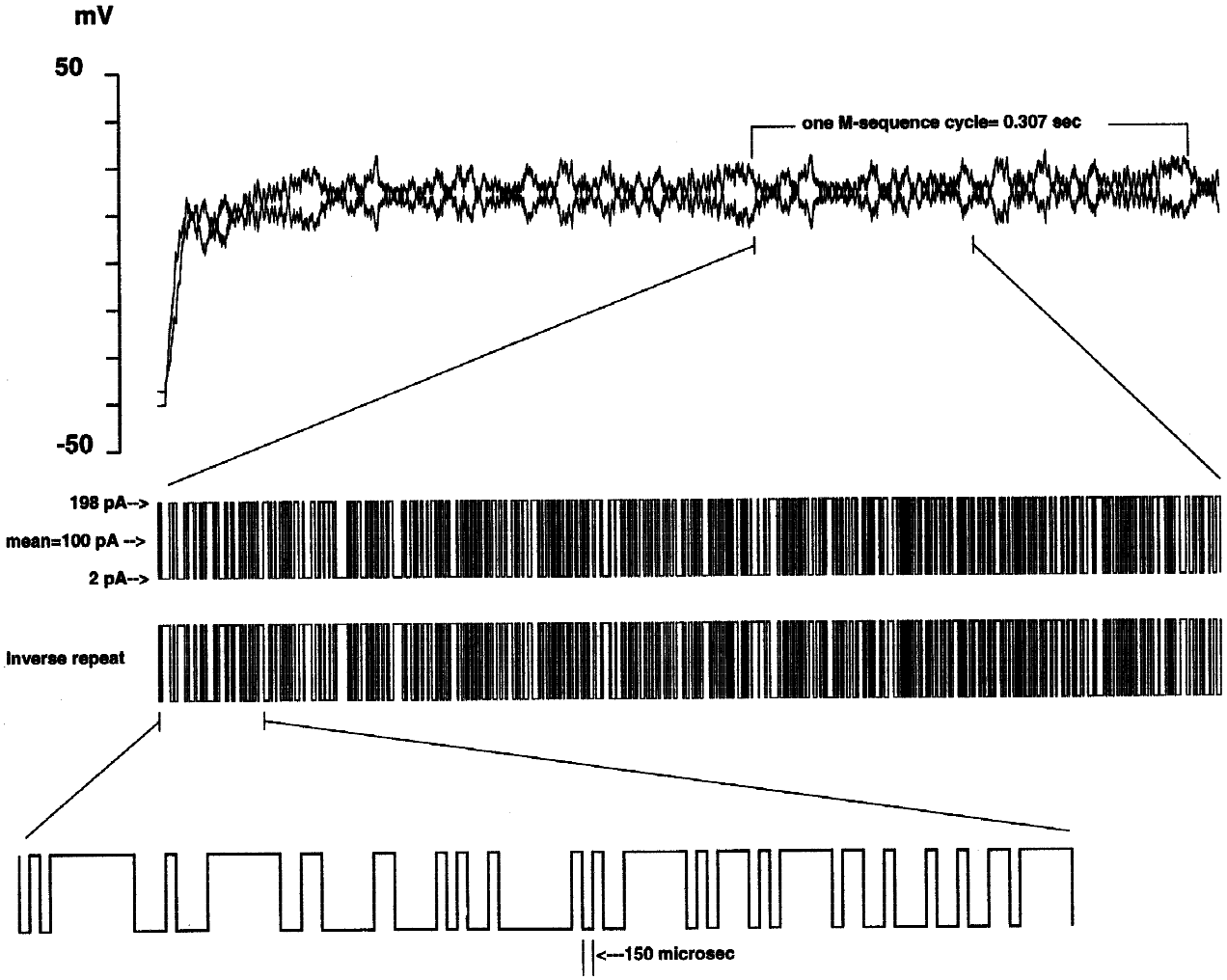

Fig. 1. Membrane potential responses to m-sequence current inputs. A bipolar cell's voltage responses to two m-sequence currents with the same mean but opposite polarities. The length of the data is about 2.5 cycles of the m-sequence, and the periodicity of the m-sequence currents is reflected in the membrane potential response. Approximately one half of a cycle of the m-sequence, corresponding to the marked time window, is shown on an expanded time scale, and a small section of the sequence is displayed on a still more expanded time scale. The m-sequence had a sampling interval T_s of 150 μs, a current scale factor of $\alpha = 98$ pA, and a mean of $\mu = 100$ pA.

resistance would be distributed over the first several data points. This "smearing" is due to the limited frequency response of recording system, which was set at 3 kHz (and T_s for the m-sequence currents ranged from 100 μs to 1000 μs).

More importantly, a real neuron differs from the model neuron in that it contains several non-Ohmic conductances, and its V–I operating curve is generally not a straight line. Characterizing the dynamics of such a neuron requires application of m-sequence currents with several mean levels (we used, typically, -25, -3, 0, 3, 7, 15, 25, 50, and 75 pA). Each m-sequence run involved application of an inverse repeat pair (with identical mean μ but opposite polarity in scale factor α) of m-sequence currents. M-sequences of different means were applied in a pseudorandom order in which high and low mean levels were interleaved to avoid any systematic trend that might result from a consistent order.

We derived several quantities from each estimated impulse response: (1) Gain (in GΩ or mV/pA) is the frequency-dependent incremental voltage response to a unit incremental input current. We examined two kinds of gain. "Static gain" is the gain for a sustained input increment and is the area under the impulse response curve. "Maximum gain" is the maximum amplitude of the transfer function (i.e. the Fourier Transform of impulse response). The two gains are the same for low-pass systems, but the maximum gain exceeds the static gain for high-pass or band-pass systems. (2) Time constant (in ms) was obtained by fitting the "initial segment" of impulse response to an exponential function (the "initial segment" was defined, arbitrarily, as ending at the point at which the integral of the impulse response equaled two thirds of the integral of the impulse response between $t = 0$ and its first zero crossing). (3) Capacitance and specific capacitance were calculated as specified in Results section.

Programs were written in C++ and Postscript II for analysis of data from m-sequence experiments, descriptive statistics, and computer simulations. Algorithms for exponential curve-fitting, Fast Fourier Transform, and integration of normal differential equations were taken from Press et al. (1992).

Results

For each of the presented results, we have at least three cells with similar data.

Bipolar cells' steady-state current–voltage relationship

Bipolar cells were identified by the distinctive morphological feature, the Landolt club. In intact retina of tiger salamanders, bipolar cells vary in the shape and size of soma, in the thickness of dendrites, and in the size (or absence) of Landolt's club (Hare et al., 1986). We recorded only from cells that had a prominent enlargement toward the end of their (presumed) primary dendrites (Figs. 2A–2D).

Fig. 3A shows current responses to voltage-clamp pulses and Fig. 3B the steady-state *I–V* curve. A relatively simple set of currents was seen across all bipolar cells. Predominant is an outward current, which can be reduced by TEA, quinidine, and quinine (Mao, 1996) and thus is most likely carried by potassium. A hyperpolarization-activated inward current was seen in many, but not all, bipolar cells. This current was blocked by extracellular cesium and enhanced by an increase in extracellular potassium (Mao, 1996). The *I–V* curve also reveals a leakage conductance in the voltage range (*ca.* −50 mV to −30 mV) where neither the outward nor the inward current is appreciably activated.

Voltage responses to depolarizing currents contain an initial, transient peak, and the time to peak was progressively shortened with increasing depolarization (Fig. 3C). The steady-state *V–I* curve (Fig. 3D) is the steepest at resting potential (i.e. for clamp current 0 pA), and levels off at more depolarizing currents. For hyperpolarizing currents, an inward rectification of the membrane voltage was observed in some cells. The inward rectification was eliminated by extracellular cesium (data not shown).

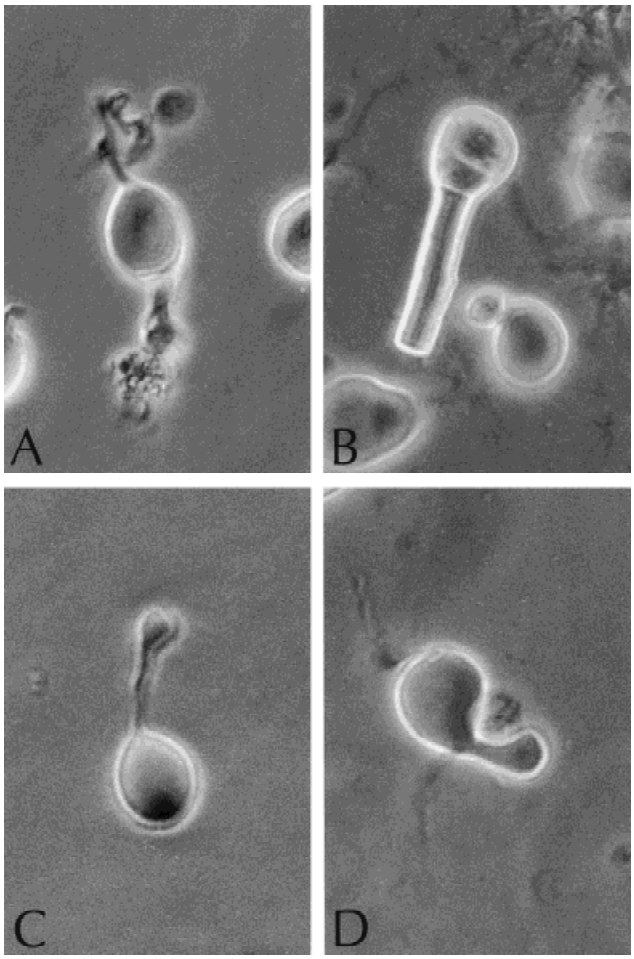

Fig. 2. Isolated retinal cells. Each of the panels A–D shows a bipolar cell dissociated from tiger salamander retina. The bipolar cells were recognized by the Landolt club, which is an enlargement of their dendrites. Panel B also shows a rod photoreceptor. The bipolar cells in these panels have a cell body diameter of approximately 15 μm.

Bipolar cells' impulse responses depend on mean currents

To study the dynamics of the bipolar cells, we applied m-sequence currents of various means to estimate the cells' impulse responses. We soon learned in pilot experiments that the bipolar cells' response gain and speed vary substantially with the mean current. Therefore, for mean currents which were customarily associated with a large gain, the scale factor α was reduced to prevent wide excursions in membrane potential. Longer T_s was used in these conditions. This arrangement was usually required for mean input currents close to zero (e.g. −3, 0, 3, and 7 pA). For situations where the gain was customarily low, and response fast (e.g. 15, 25, 50, and 75 pA, etc.), α was increased, and T_s reduced, to maintain an adequate signal-to-noise ratio.

Fig. 4 shows that the mean level of m-sequence currents determines impulse responses. At resting potential (0 pA), the cell has a slow impulse response. When the cell is depolarized (25 pA and 100 pA), its impulse responses become faster. In addition, an undershoot appears in the impulse responses. In this cell, the response is fast for hyperpolarizing currents (−25 pA) as well. Resting potential was estimated from 52 cells, and had a mean of -37.6 ± 14.4 mV (S.D.) ($n = 101$ because replicate runs of inverse-repeat m-sequence pairs for 0 pA were obtained in most cells).

This change in effective impulse response with mean current indicates that bipolar cells are not linear systems over the entire range of mean input currents. Nevertheless, for a given mean current (e.g. 0 pA, 7 pA, 15 pA, and 25 pA), bipolar cells behave in a linear fashion. This quasilinearity was tested by varying the scale factor α (by more than one order of magnitude). We found that the excursions of the membrane voltage were proportional to the scale factor and impulse responses did not vary with scale factor (not shown). This quasilinearity is also manifest by the near mirror-symmetry of the membrane voltage responses to the pair of the inverse repeat m-sequence currents (Figs. 1 and 4). "Linear" responses of bipolar cells were noted in intact retina of several animals (Naka et al., 1975; Ashmore & Falk, 1980; Copenhagen et al., 1983) including tiger salamanders (Capovilla et al., 1987). The results here indicate that the apparent linearity of the bipolar cells in the intact retina depends in a subtle fashion on their intrinsic membrane properties, and is only one aspect of an intrinsically nonlinear set of response properties.

Bipolar cells as adaptive filters

Fig. 5 is an overview of how a bipolar cell's dynamics depend on the mean (μ) of the input currents. Impulse response curves (as functions of time) are plotted in an (I, V) plane, with their origins ($t = 0$) positioned according to the mean current input (I) and the measured mean voltage response (V). Several currents (−25 pA,

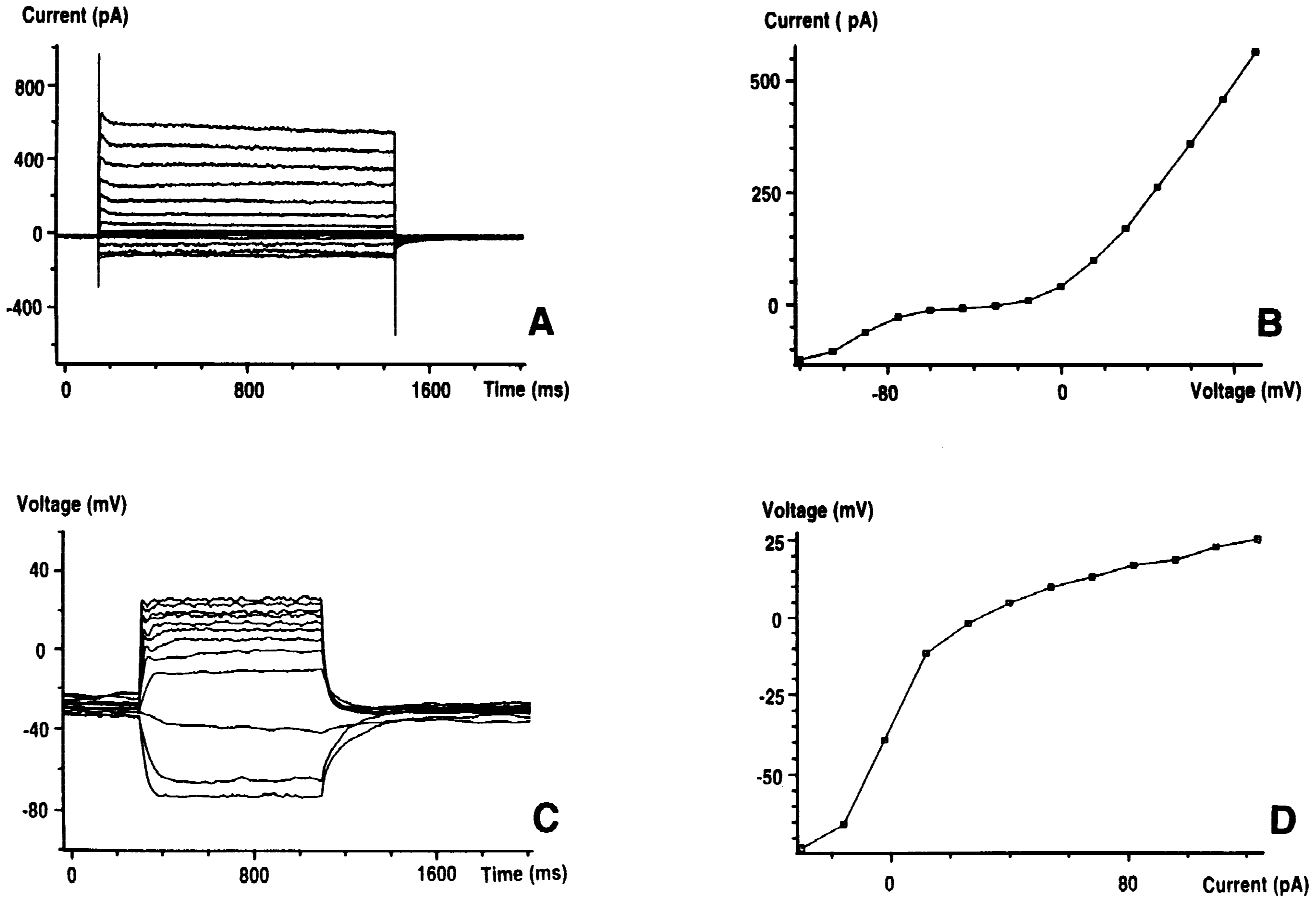

Fig. 3. *I–V* curves from voltage-clamp and current-clamp experiments. Panel A: Superimposed current responses of a bipolar cell to multiple voltage commands. Panel B: *I–V* curve obtained from the steady-state currents in Panel A. Panel C: Superimposed membrane potential responses of the same bipolar cell to multiple current commands. Panel D: *V–I* curve obtained from the steady-state voltages in panel C.

0 pA, 25 pA, and 75 pA) were applied on two separate occasions to assess the stability of the preparation. The measured mean voltage responses and the impulse responses were similar (though not identical) on each presentation. Note also that on each of the repeated runs, different sampling intervals (T_s) were used, as evident by the differences in the length of the estimated impulse responses on the two occasions. However, the shape and size of the impulse responses did not depend on T_s. Thus, isolated bipolar cells behave as quasilinear adaptive filters, whose gain and dynamics are regulated by the mean input.

The characteristic changes seen in Fig. 5 can be summarized by several quantities derived from the impulse responses. Fig. 6A shows maximum gain (defined in Methods) as a function of mean injected current: it has a sharp descent from a maximum value near resting potential, and a more gradual decline with more depolarizing currents. Time constant behavior is similar to that of the maximum gain (Fig. 6B), as is the behavior of the static gain (not shown). The reductions in gain and time constant by hyperpolarizing currents were caused by the activation of a Cs^+- and K^+-sensitive inwardly rectifying current (since the reductions were eliminated by extracellular cesium and modified by potassium). This reduction of gain and time constant was not always observed, presumably due to the lack of the inwardly rectifying current in some cells. However, in every cell in which the gain decreases with hyperpolarizing currents, the time constant does too, and *vice versa*. Fig. 6 thus indicates a tradeoff between gain and speed in the bipolar cell's intrinsic dynamics. Of the 52 cells, the mean of maximum gain is 4.95 ± 2.05 mV/pA (S.D.) and the mean of peak time constant is 99.7 ± 52.1 ms (S.D.). Of note, for a first-order, low-pass system (which is a good approximation for the bipolar cell at resting potential), a time constant of 100 ms corresponds to a corner frequency of 1.6 Hz.

A qualitative change in the impulse responses, as already mentioned, was the emergence of an undershoot for depolarizing mean currents (Figs. 4 and 5). The presence of undershoot usually implies that, in the frequency domain, maximum gain occurs at a frequency which is not zero. To examine if this was indeed the case, we calculated transfer functions, $H(f)$, from the impulse responses $h_n = h(nT_s)$ $(0 \le n < 2^M - 1)$. The amplitude and phase of $H(f)$ are shown in Figs. 7A and 7B. At resting potential, the transfer functions resemble that of a first-order, low-pass system: the amplitude decreases monotonically and approaches a straight line with slope −1 (Fig. 7A) and the phase approaches −90 deg (Fig. 7B). With depolarization, amplitude was reduced (flattened) at low frequencies, but less so (indeed relatively enhanced, as reflected by a peak) at higher frequencies. With increasing depolarization (from 15 pA to 100 pA), the frequency at which the transfer function amplitude reaches maximum becomes higher.

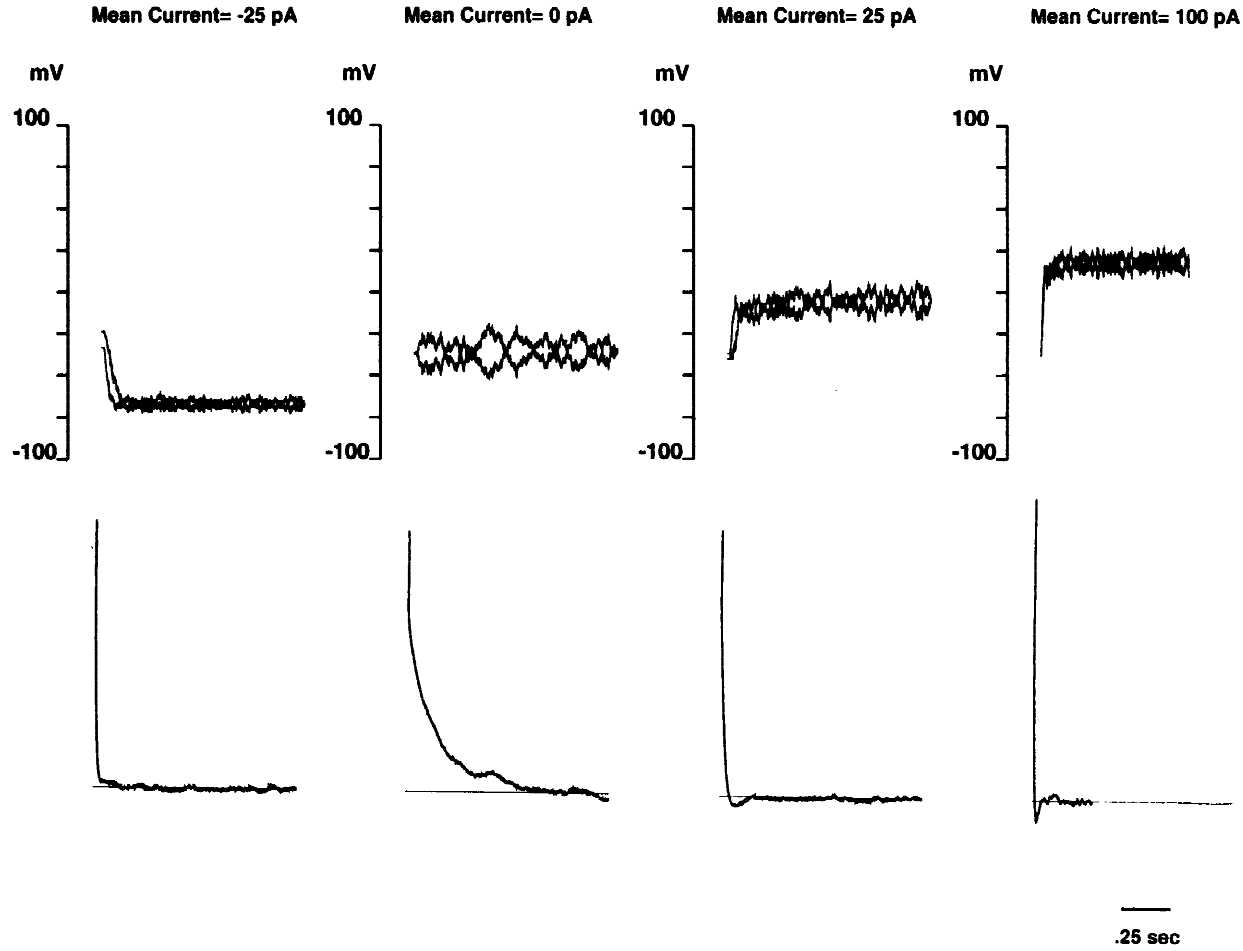

Fig. 4. Membrane potential response to an m-sequence depends on the mean current. Upper panels show a bipolar cell's voltage responses to m-sequence currents with means of −25, 0, 25, and 100 pA. Lower panels show corresponding impulse responses (estimated by a crosscorrelation between the responses and the m-sequence input). With increasing mean currents, the mean membrane potentials become progressively depolarized. At resting potential (0 pA), the impulse response is slow, near-exponential, and the area under the curve (the static gain) is large; with depolarization (25 and 100 pA), the impulse response becomes faster, and the area under the curve is smaller. The presence of an undershoot further accelerates the declining phase and reduces the static gain. In this cell, hyperpolarization (−25 pA) also speeds up impulse response, yet causes no undershoot. The spike-like segment at $t = 0$ in each of the four impulse responses represents the effect of the electrode resistance.

With depolarization, the phase lag decreases and even becomes phase lead at some frequencies. The frequency range in which the phase lead occurs becomes higher and broader with increasing depolarization. However, all of the transfer functions have a common boundary in the high-frequency region: an asymptote with slope −1 limits all the transfer function amplitude curves; for phase, the −90 deg line is the common asymptote.

To measure the frequency at which transfer function amplitude reaches maximum, we calculated the index f_{max}, defined by

$$f_{max} = \frac{\int |H(f)|^p f \cdot df}{\int |H(f)|^p \cdot df} \tag{4}$$

When p is large, this measurement puts a heavy weight on the precise frequency at which the transfer function reaches its maximum; with small p, the index becomes more resistant to noise in the estimated transfer function. We used $p = 20$ as a compromise between the sensitivity to the detailed shape of transfer function and resistance to noise. As Fig. 7C shows, f_{max} increases with increasing depolarization, while at the resting potential, f_{max} is near zero.

Membrane capacitance

Capacitance, according to eqn. (3), can be estimated as the reciprocal of the amplitude of impulse at $t = 0$ (ignoring the effect of R_s). This method is based on the electric properties of a parallel capacitance, and is generally valid even for impulse responses for which eqn. (3) is not a good fit (e.g. when the impulse responses contain an undershoot). Due to the "smearing" effect of R_s resulting from the nonideal recording system, when estimating the capacitance, the first three data points were substituted with values extrapolated from later data points. From each impulse response, one estimate, $\hat{C}$, can be obtained. Thus, data from each recording yields multiple capacitance estimates. We found that the individual

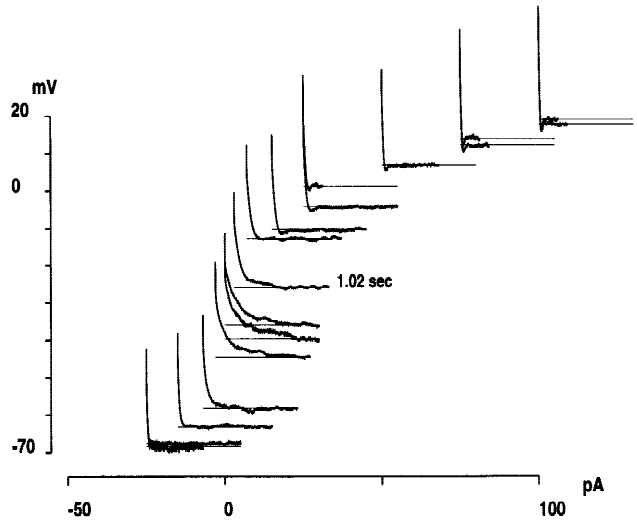

Fig. 5. The bipolar cell as an adaptive filter. For the same cell as shown in Fig. 3, impulse responses were estimated from m-sequence runs with a range of mean currents. For each mean current, the impulse response is plotted as a function of time. The coordinates of the origin of each impulse response represent the mean current (abscissa) and mean voltage response (ordinate). All the impulse response curves have the same amplitude scale and time scale. The full length of the time axis for the impulse responses is 1.02 s.

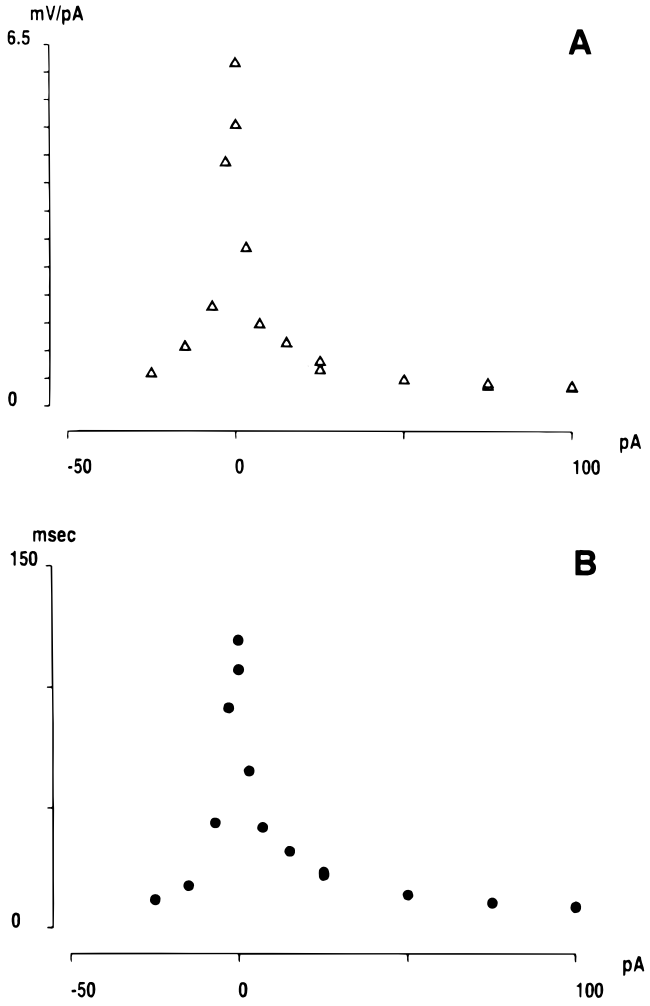

Fig. 6. Gain and time constant as functions of mean input current. Gain (in mV/pA) and time constant (in ms) were calculated from the impulse responses shown in Fig. 5. Panel A: Maximum gain as a function of mean current. The gain is largest at the resting potential and decreases with depolarization and (in this cell) hyperpolarization. Panel B: Time constant as a function of mean current. Depolarization and (in this cell) hyperpolarization reduce time constant.

estimated values $\hat{C}$ depended modestly but systematically on the sampling intervals (T_s) of the m-sequences: the longer the T_s, the larger the $\hat{C}$. Moreover, the relationship of $\hat{C}(T_s)$ to T_s is steeper for smaller T_s and flatter for larger T_s (not shown). To understand this, first consider the impulse response of an *RC* circuit, with the assumption that impulse responses estimated from applying m-sequence (with time interval T_s) is equivalent to the responses to a literal impulse (with duration T_s and amplitude $1/T_s$). The impulse response consists of two phases (both with time constant $\tau = RC$): a rising phase until $t = T_s$, followed by a falling phase. The voltage at $t = T_s$ is $V(T_s) = (R/T_s)\cdot\{1 - \exp[-T_s/(RC)]\} = (1/C)\cdot[1 - T_s/(2\tau) + o(T_s)]$. ($o(T_s)$ denotes a quantity whose ratio to T_s approaches 0 in the limit that T_s approaches 0.) Capacitance can be estimated as $\hat{C} = 1/V(T_s) = C/[1 - T_s/(2\tau) + o(T_s)] \approx C\cdot[1 + T_s/(2\tau)]$. This relationship shows that the best estimate for capacitance would be the extrapolated value of $\hat{C}$ at $T_s = 0$. Furthermore, $\hat{C}$ will always be an overestimation of C, and the bias is proportional to T_s/τ. In an actual bipolar cell, however, the effective time constant τ depends heavily on the mean current, for which reason we adjusted the sampling interval T_s of the m-sequence so that it was larger for slow responses ($1/\tau$ small), and smaller for fast responses ($1/\tau$ large). Thus, the relationship of $\hat{C}(T_s)$ to T_s has a steeper slope for smaller T_s and a flatter slope for larger T_s. For these reasons, we used a quadratic curve $c_0 + c_1\cdot T_s + c_2\cdot T_s^2$ (determined by least squares) to extrapolate the set of measurements of $\hat{C}$ to a final estimate of capacitance corresponding to $T_s = 0$ μs. The mean of the estimates for recordings thus analyzed was 10.2 ± 3.6 pF(S.D.), $n = 81$.

For calculating specific capacitance, the membrane area of a bipolar cell was estimated by numerical surface integration. The cells were idealized as an ellipsoid with three axes, of lengths *a*, *b*, and *c*. Axes *a* and *b* were measured from the photomicrograph of each cell. The third axis (perpendicular to the plane of the photograph), *c*, was assigned a value based on two assumptions: first, a cell settles to a position with its longest axis (*a*) parallel to the coverslip bottom; second, the cell tends to be flattened as it adheres to the coverslip. Under the assumption that $c = 2/3\ \min(a,b)$, the specific capacitance was 1.50 ± 0.61 μF/cm^2 (S.D.), $n = 81$. Under the assumption that $c = \min(a,b)$, the specific capacitance was 1.20 ± 0.48 μF/cm^2 (S.D.), $n = 81$.

Blocking outward current alters bipolar cell's dynamics

Tessier-Lavigne et al. (1988) used choline in pipette to block the (largely potassium) outward currents in salamander bipolar cells. Barium also blocks the potassium channel from either side of the membrane (Armstrong et al., 1982). In the present study, we found that these agents reduced substantially, and in many cases completely, the outward currents in isolated bipolar cells. We then proceeded to see how these agents affect the bipolar cells' dynamics.

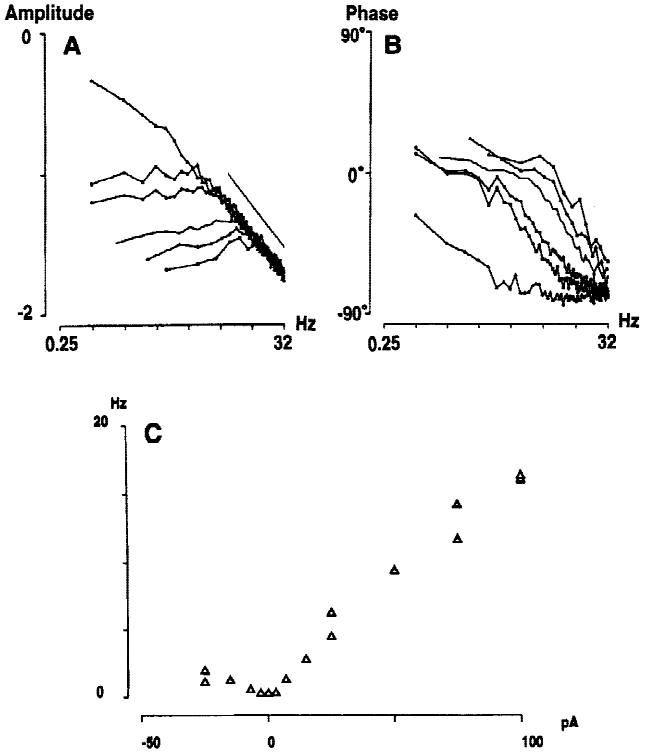

Fig. 7. Transfer function (amplitude and phase) and peak response frequency as functions of input current. Transfer function amplitude (Panel A) and phase (Panel B) calculated from the Fourier Transform of impulse responses shown in Fig. 5 at representative mean currents: 0, 15, 25, 50, 75, and 100 pA. Frequency scale is 0.25 to 32 Hz in octave steps. Amplitude curves (Panel A) are arranged with the smallest mean current on the top (greatest gain), and are plotted on a $\log_{10}$ scale, with 0 corresponding to 10 mV/pA and -2 corresponding to 0.1 mV/pA. Phase curves (Panel B) are arranged with the smallest mean current on the bottom (most phase lag), and the ordinate scale represents the phase shift in degrees. Generally, amplitude is progressively reduced by depolarization, but more so at low than at high frequencies. For 15, 25, 50, 75, and 100 pA, there is a peak in the amplitude of the transfer functions at a nonzero frequency, signifying band-pass behavior. Near resting potential, there is a consistent phase lag which increases with frequency. Depolarization reduces the phase lag, and indeed at some frequencies there is a phase lead (>0 deg), which is also a sign of band-pass behavior. The phase lead becomes more pronounced with increasing depolarization. All the phase curves also converge toward -90 deg at high frequency range. Panel C: f_{max}, calculated by eqn. (4), increases with the mean current, which indicates a high-frequency enhancement of the bipolar cell's frequency response.

Fig. 8 shows results from potassium replacement by choline in the pipette. Immediately after a whole-cell, patch-clamp configuration was established on a bipolar cell, a voltage pulse (40 mV for 1.2 s) was repeatedly (at 15-s intervals) applied. Outward currents were reduced (Fig. 8A). The time course of the reduction, approximately exponential, may reflect the diffusion of choline into the cell (Fig. 8B). After the blockade was complete, impulse responses were measured, and showed the dynamics of a passive *RC* circuit: the static *V–I* curve is linear, impulse responses are independent of the mean currents (Fig. 8C), and transfer functions are low-pass (Fig. 8D). The impulse responses show no undershoots.

Similar experiments were carried out with 10 mM $BaCl_2$ in the pipette (replacing equal osmolar KCl). Repetition of a voltage command (40 mV for 1.2 s) at 5-s intervals resulted in progressive reduction of the outward currents (Figs. 9A and 9B). Barium occludes potassium channels, which requires an open channel (Armstrong et al., 1982). Therefore, the time course of the outward current reduction may reflect the fraction of potassium channels which had not already been occluded by the barium ion.

We observed how the changes in dynamics evolved while the blocking effect of barium was taking place. Upon the formation of the whole-cell, current-clamp configuration, an m-sequence current (25 pA) was repeatedly injected into the bipolar cell from a pipette containing 3 mM $BaCl_2$. Estimated impulse responses are plotted in a (V, t) plane: V is mean voltage and t is the time, in seconds, after the first application of the m-sequence (Fig. 9C). An undershoot is evident initially, but soon disappears in the successive impulse responses. Changes in the shape of the impulse responses are substantial: the cell becomes progressively depolarized, yet the impulse response becomes slow and dynamics become low-pass as the undershoot disappears. Thus, the intrinsic regulation of bipolar cells' gain and dynamics involves a Ba^{2+}-sensitive conductance. This experiment also shows that the change in dynamics is not due to a change in membrane potential *per se*.

A brief consideration of kinetics

Across the experimental conditions and recordings, the kinetics of the outward current varied in several respects. Under normal ion conditions, voltage-dependent inactivation was observed in most of the bipolar cells. However, the inactivation did not appear to change the impulse response during the time scale the adaptive behavior was studied, because inactivation occurred at a time scale much longer than activation (data not shown). The inactivation of the potassium current induced by internal barium is an established observation (Armstrong et al., 1982). This was seen in Fig. 9A. However, the change in dynamics (as shown in Fig. 9C) was probably due more to the substantial reduction of the potassium conductance than to the change in its kinetics. A second variation in kinetics was that the outward current often contained more than one component. In addition to a delayed-rectifier-like current, which was present in all bipolar cells studied, there was often an A-channel-like component, as seen by a notch in the current traces shown in Fig. 3A. The A-channel component did not change the adaptive behavior in gain and time constant, but it tended to reduce the band-pass nature of the impulse response (data not shown).

Computer simulations reconstruct bipolar cells' adaptive behavior

We undertook computer simulations intended to provide a qualitative understanding of the experimentally observed adaptive behavior. The model neuron (as detailed in Table 1) has a capacitance C_m, a nonspecific leakage conductance G_l, a voltage-independent potassium conductance G_{Kleak} (which largely sets the resting membrane potential), and a delayed-rectifier G_K. The model includes the minimal number of channels to capture the observed behavior for voltage above the resting potential. The model neuron is "minimalist" also in that it includes only channels which are the most common and most indispensable—the delayed-rectifier, arguably, is the most widespread and basic channel for all neurons (Rudy, 1988). The model is consistent with experimental evidence we presented that a voltage-dependent potassium conductance underlies the adaptive behavior observed in this voltage range. The simulations reproduced, with satisfactory fidelity, bipolar cells' observed quasilinear adaptive filter behaviors. The simulations also

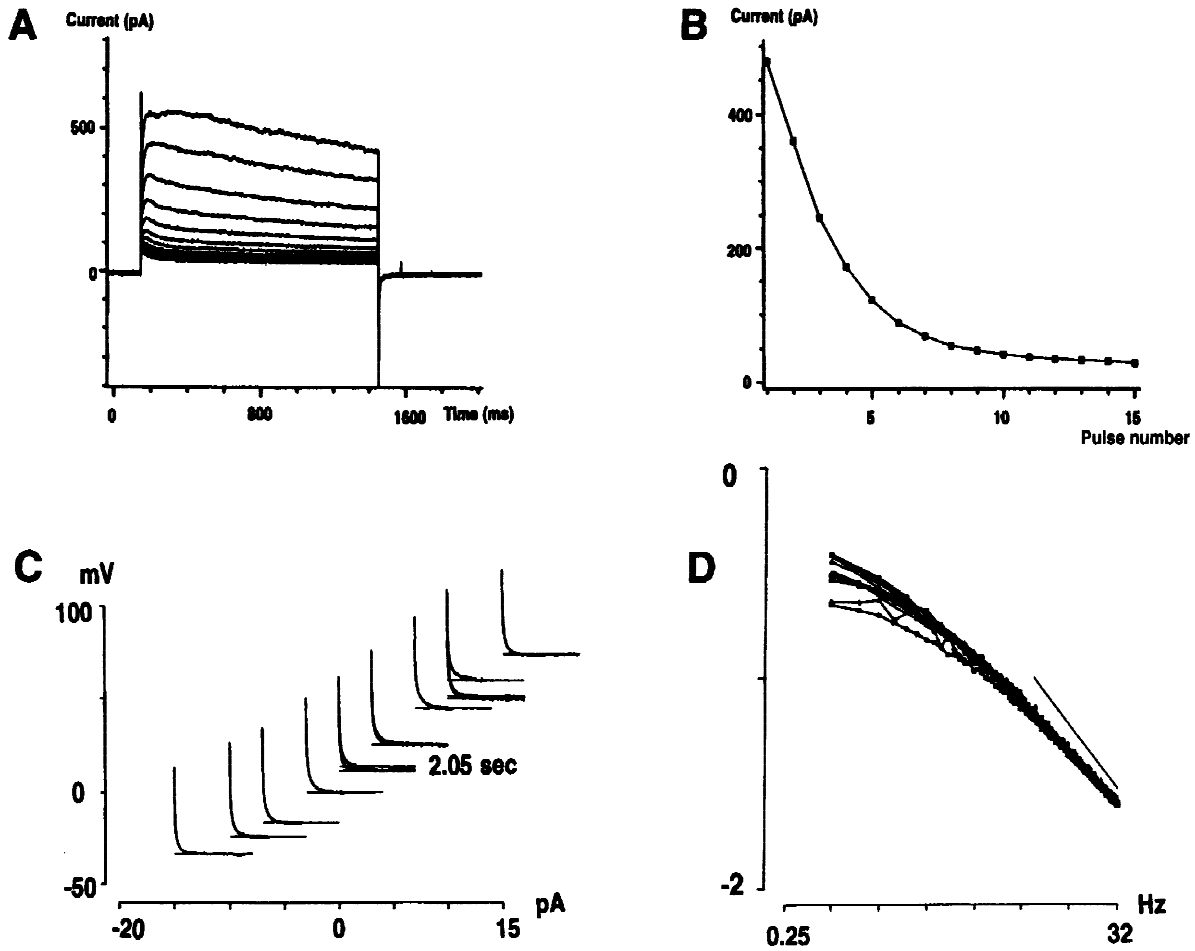

Fig. 8. Substitution of choline for potassium in the pipette alters bipolar cells' intrinsic dynamics. Panel A: Superimposed current responses of a bipolar cell to multiple applications of a 40 mV voltage pulse at 15-s intervals. Pipette included 120 mM choline Cl (replacing KCl). The currents decrease with successive applications of the pulse. Panel B: The time course of the outward current reduction measured by the current near the end of each voltage pulse (at *ca.* 1400 ms). The abscissa is the pulse number (the interval between consecutive pulses is 15 s). The roughly exponential time course may reflect the time process by which the choline in the pipette diffused into the cell. Panel C: M-sequence analysis of the bipolar cell's dynamics after the blockade of outward current by choline was complete. Impulse responses are presented in the same format as in Fig. 5. The bipolar cell behaved like a passive *RC* circuit, as indicated by the exponential form of each impulse response and the near-linear static *V–I* relationship. Panel D: Transfer function amplitude obtained from the impulse responses in panel C. Frequency scale is 0.25 to 32 Hz in octave steps. Amplitudes are plotted on a $\log_{10}$ scale, with 0 corresponding to 10 mV/pA and -2 corresponding to 0.1 mV/pA.

provided insight into channel parameters which are less accessible to observation.

Model voltage responses to m-sequence currents were calculated for two mean current levels, 0 pA and 50 pA, and impulse responses were estimated. Results are shown in Figs. 10A and 10B (for 0 pA) and Figs. 10C and 10D (for 50 pA). Note different scales for these panels. For each mean current level, the voltage responses to the inverse repeat pair are nearly symmetric about the mean voltage (upper traces in Figs. 10A and 10C), indicating quasilinearity. The lower traces in Figs. 10A and 10C are the time courses of parameter n^4, in the Hodgkin-Huxley model of the delayed-rectifier, in response to the m-sequence currents. For the mean current 0 pA, n^4 is close to 0, corresponding to a virtually zero open probability (thus the conductance) of the delayed-rectifier. For the mean current 50 pA, n^4 increases. Estimated impulse responses of voltage for 0 pA and 50 pA are plotted, respectively, in the upper left subplots of Figs. 10B and 10D. The lower left subplots of Figs. 10B and 10D are impulse responses of n^4 for 0 pA and 50 pA, respectively. For the mean current 0 pA (i.e. at resting potential), the voltage impulse response has a peak value at $t = 0$, then declines with a near-exponential time course (Fig. 10B upper left subplot). The impulse responses of n^4 (thus the conductance) of the delayed-rectifier rises to a peak, then declines to zero (Fig. 10B lower left subplot). Overall, the impulse responses of voltage and of n^4 are not much different in shape, although the former slightly leads the latter. By contrast, for the 50 pA mean current, the impulse responses of both voltage and n^4 (Fig. 10D upper and lower left subplots, respectively) decline to zero with a time course much faster than for the 0 pA mean current. (Note five-fold difference in time scale.) Moreover, both impulse responses have an undershoot, followed by diminishing wavelets which indicate damped oscillations. But the impulse response of voltage has a substantial phase lead relative to that of n^4. This phase lead is key to the emergence of undershoot (Mao, 1996).

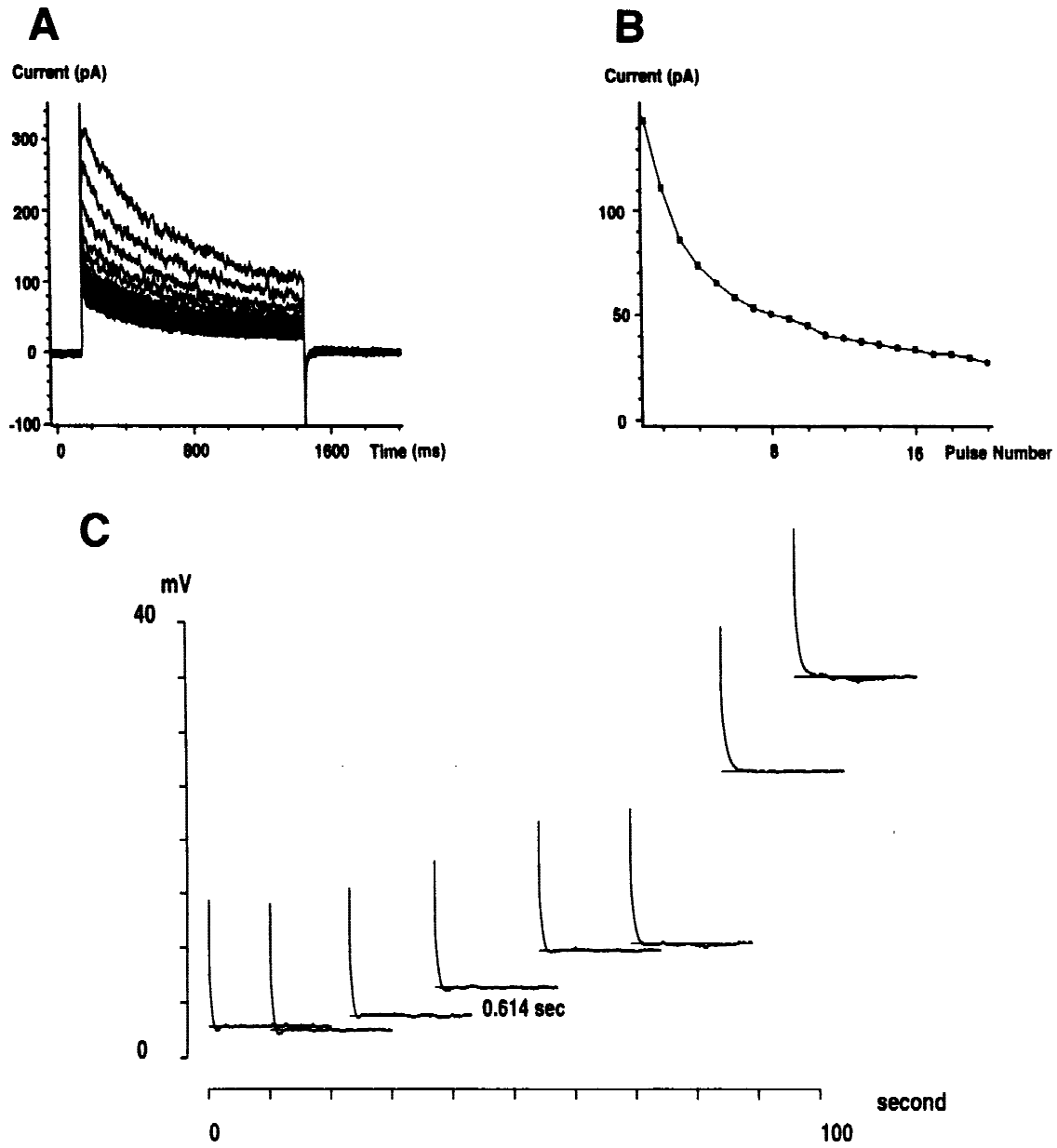

Fig. 9. Changes in dynamics induced by the potassium channel blocker Barium. Panel A: Superimposed current responses of a bipolar cell to a 40-mV voltage pulse applied every 5 s. Pipette included 10 mM $BaCl_2$. Barium affected outward currents in two aspects: it reduced the overall outward current with each successive voltage pulse, and it induced an inactivation within the duration of each application. Panel B: The time course of the diminishing outward currents. The abscissa is the pulse number (consecutive pulses are separated by 5 s) and the ordinate is the current near the end of each voltage pulse. Panel C: (On another bipolar cell) The time course of the Ba^{2+} (3 mM) induced dynamics changes, as studied by the repetitive application of an m-sequence current (with 25 pA mean) after the current-clamp mode was established. Estimated impulse responses are plotted in a (V,t) plane: V is the mean membrane voltage and t is the time at which the m-sequence currents (relative to the first one) were applied. Note the change from fast impulse responses with undershoots to slow impulse responses with monotonic declines.

Alternatively, impulse responses were obtained by directly calculating the model neuron's responses to a literal impulse. The impulse responses of voltage are shown in the upper right subplots of Fig. 10B (0 pA) and Fig. 10D (50 pA), and those of n^4 are in the lower right subplots of these panels. These directly calculated impulse responses are indistinguishable from those estimated by the m-sequence method, which is another indication of quasilinearity.

Fig. 11 is an overview of the model neuron's voltage impulse responses at various mean currents. Near resting potential, the impulse response is slow and low-pass. Depolarization increases the speed of the responses and leads to the appearance of undershoots in the impulse responses. The static gain (the area under the impulse response curve) is maximum near resting potential and is reduced with depolarization. Thus, a delayed-rectifier conductance underlies the adaptive behavior we observed experimentally.

Table 1. *Simulation parameters of a model neuron*

	Value	Reversal potential	Kinetics
C_m membrane capacitance	10 pF	NA	NA
G_{ns} nonspecific leakage conductance	0.15 $G\Omega^{-1}$	0 mV	Ohmic
G_{Kleak} voltage-independent potassium conductance	0.15 $G\Omega^{-1}$	−90 mV	Ohmic
G_K voltage-dependent potassium conductance	5 $G\Omega^{-1}$	−90 mV	Hodgkin-Huxley (1952) type delayed-rectifier.[a]

[a]Forward rate: $\alpha = a_1(V - b_1)/\{1 - \exp[(b_1 - V)/c_1]\}$. $a_1 = 0.005$ ms^{-1}, $b_1 = -55$ mV, $c_1 = 24$ mV. Backward rate: $\beta = a_2(b_2 - V)/\{1 - \exp[(V - b_2)/c_2]\}$. $a_2 = 0.025$ ms^{-1}, $b_2 = -45$ mV, $c_2 = 12$ mV. $n = \alpha/(\alpha + \beta)$, $\tau = 1/(\alpha + \beta)$. Open probability: n^4. $g_K = G_K \cdot n^4$.

Discussion

Intrinsic dynamics are similar among bipolar cells

There is a relatively large scatter of the estimated resting potential (−37.6 ± 14.4 mV (S.D.), $n = 101$), gain (4.95 ± 2.05 mV/pA (S.D.), $n = 52$), time constant (99.7 ± 52.1 ms (S.D.), $n = 52$), and capacitance (10.2 ± 3.6 pF (S.D.), $n = 81$) among the bipolar cells we recorded. However, scattergrams (not shown) of several combinations of these parameters (time constant *vs.* gain, gain *vs.* resting potential, capacitance *vs.* gain, and capacitance *vs.* resting potential) did not suggest the presence of more than one population. Therefore, in terms of the intrinsic dynamics, the differences among bipolar cells we recorded appear to indicate a continuum of properties, rather than separate subtypes. In terms of the ON–OFF dichotomy, evidence suggests that the dissociation procedure which we adopted did not select one type of bipolar cells over the other (Hirano & MacLeish, 1991). Therefore, even though we did not classify the bipolar cells as ON or OFF according to their responses to glutamate, it appears that our findings of adaptive filtering apply to both kinds of cells, since this behavior was present in all the cells studied.

Further considerations of the roles of intrinsic dynamics in the ON- and OFF-bipolar cells' responses are bound to be somewhat speculative. However, there is some similarity between an ON-bipolar cell's response to light and an OFF-bipolar cell's response to the decrease of light: in both cases, the change is a depolarization resulting from an increase of a conductance. For the ON-bipolar cell, it involves a cGMP-gated conductance, and for the OFF-bipolar cell, it is an ionotropic glutamate-receptor channel (Shiells et al., 1981; Nawy & Jahr, 1990; Hirano & MacLeish, 1991; Shiells & Falk, 1992). Therefore, under physiological circumstances, the intrinsic adaptive filtering we have observed likely modifies the light-ON response of the ON-bipolar cell and the light-OFF responses of the OFF-bipolar cell in a similar manner. Due to the two different channel mechanisms for the ON- and OFF-bipolar cells (the former involves an internal messenger system), there are detectable temporal differences in the two types of bipolar cells' responses (Kim & Miller, 1993). Difference in response speed in ON- and OFF-pathway was also noted in cat (Victor, 1988). Whether the intrinsic adaptive filtering process contributes to the differences in the temporal responses of ON- and OFF-bipolar cells, or actually results in the reduction of these differences, is an open question. Our ability to draw inference concerning the functional role of the adaptive filtering we observed is limited by the incomplete knowledge of what the resting potential is *in vivo*. For instance, since transmitter release from photoreceptors is highest in darkness and is reduced by light, it is likely that *in vivo* the membrane potential in darkness of ON-bipolar cells is more negative, and that of OFF-bipolar cells more positive, than the resting potential we measured in isolated cells. This would lead to a situation where light first increases gain and slows down response and then speeds up response and reduces gain. Whether this happens physiologically depends on the value of synaptic conductance relative to that of the intrinsic, voltage-dependent conductance, and on the ion conditions, such as the local concentration of potassium, in which the bipolar cells are situated.

Potassium conductance and the signal processing of bipolar cells

To determine whether potassium conductance plays a role in shaping bipolar cells' response, one issue is whether the channel opens at the bipolar cells' physiological voltage range. Tessier-Lavigne et al. (1988) argued against a role for voltage-dependent potassium conductance because current fluctuations of the voltage-dependent conductance are minimal at resting potential.

The bipolar cells' physiological operating range is no more positive than −20 mV (Werblin & Dowling, 1969; Lasater, 1988). We examined in our data the membrane voltage at which outward currents are activated and membrane voltages at which undershoots first appear. The outward (potassium) currents activated around −30 mV. Undershoots were first seen at voltages ranging from −10 mV to −25 mV in the majority of cells ($n > 40$), and between −25 mV and −40 mV in eight cells. Thus, for most cells the band-pass behavior was near the border of normal physiological range. However, transfer properties were studied, by necessity, at a discrete set of mean currents. Due to the fact that the gain is high near resting potential, the discrete sampling of mean currents necessarily produces a conservative (positive) bias in our estimation of the onset voltage of band-pass behavior.

A known characteristic of the synaptic transmission from photoreceptors to second-order neurons is that only a small part of the photoreceptor's voltage signals is transmitted, resulting in "signal clipping," indicated by an apparent rectification in the response of the second-order neurons (Attwell et al., 1987; Belgum & Copenhagen, 1988; Wu & Yang, 1992). The mechanism for this is believed to be presynaptic (Bader et al., 1982; Attwell et al., 1987). However, a postsynaptic mechanism is suggested by results from retinal slices of tiger salamanders: the rectification of ON-bipolar cells' voltage light responses occurred at a light intensity 1–2 orders of magnitude lower than current light responses, and this

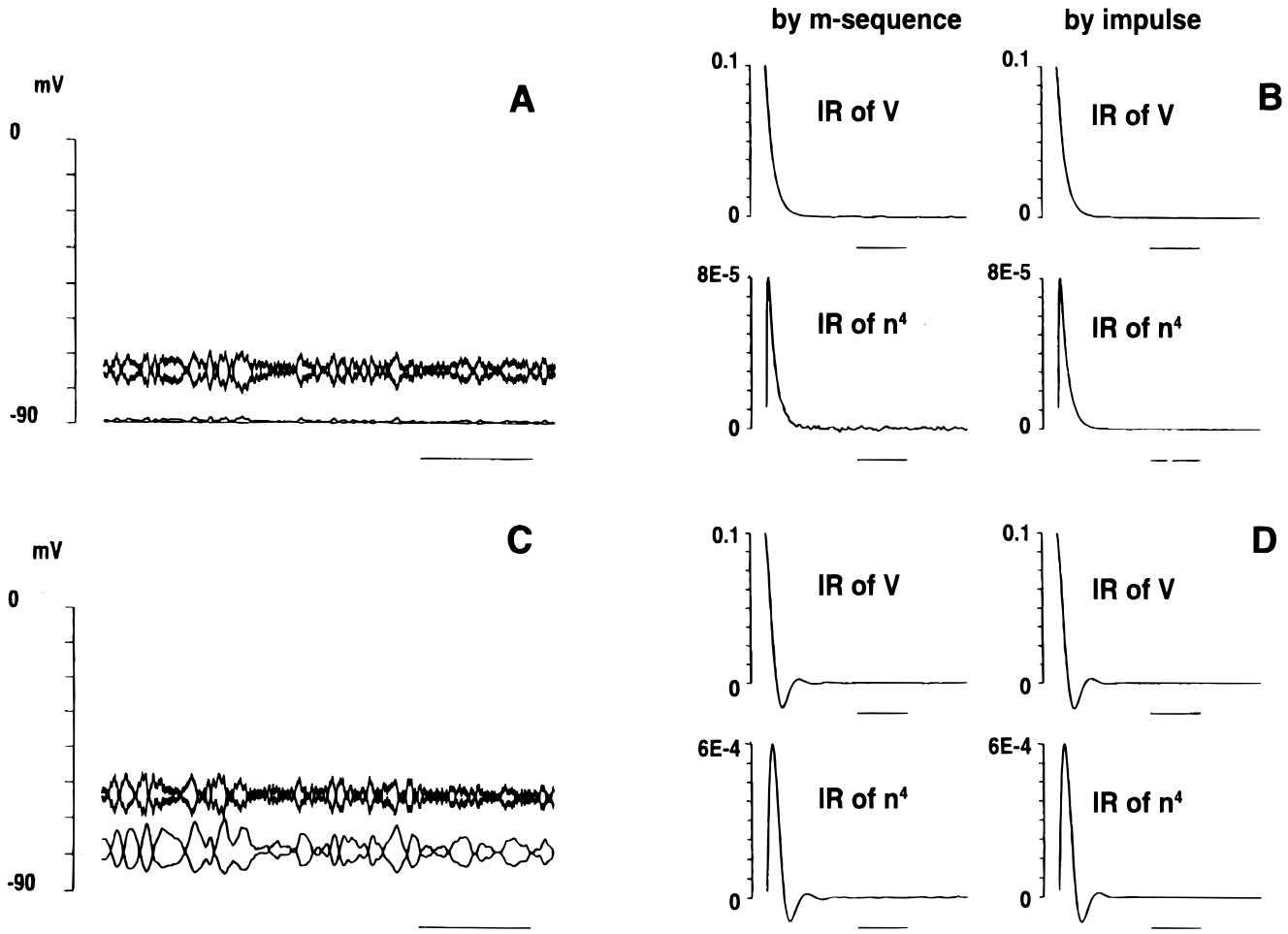

Fig. 10. Simulation: impulse responses of the model neuron. Panel A: Responses of the model neuron (Table 1) to an inverse-repeat pair of m-sequence currents with mean 0 pA. The two upper traces are membrane voltage responses and the two lower traces (close to zero) are variable n^4 of the Hodgkin-Huxley model. Amplitude scale for voltage is -90 mV to 0 mV. Amplitude scale for n^4 is from 0 to 1. The time scale bar is 250 ms. Panel B: Comparison of impulse responses estimated from responses to an m-sequence of mean 0 pA (left) and from a literal impulse (amplitude 100 pA and width 50 μs) superimposed on a current of 0 pA (right). IR stands for impulse response. Upper subplots: impulse response of membrane voltage (IR of V). Amplitude scale is 0 to 0.1 $\text{mV}\cdot\text{pA}^{-1}\cdot\text{ms}^{-1}$. Lower subplots: impulse responses of n^4 (IR of n^4). Amplitude scale is 0 to 8×10^{-5} $\text{pA}^{-1}\cdot\text{ms}^{-1}$. Time scale bar for all subplots of Panel B is 125 ms. Panels C and D: Similar to Panels A and B, but the mean current is 50 pA. Panel C: membrane voltage responses and responses of the Hodgkin-Huxley variable n^4 to the m-sequence. Amplitude scale for voltage is -90 mV to 0 mV. Amplitude scale for n^4 is from 0 to 1. The time scale bar is 50 ms. Panel D: Impulse responses estimated from an m-sequence of mean 50 pA (*left*) and from a literal impulse (amplitude 50 pA and width 50 μs) superimposed on 50 pA (right). IR stands for impulse response. Amplitude scale for the upper subplots (voltage) is 0 to 0.1 $\text{mV}\cdot\text{pA}^{-1}\cdot\text{ms}^{-1}$, amplitude for the lower subplots (n^4) is 0 to 6×10^{-4} $\text{pA}^{-1}\cdot\text{ms}^{-1}$. Time scale bar for all subplots of Panel D is 25 ms.

rectification was eliminated by TEA in the recording pipette (Lasansky, 1992). Membrane potential rectification was also seen in the *I–V* curve of ON-bipolar cells in retinal slices (Tian & Slaughter, 1995).

From the above considerations, we suggest that, at least for the photoreceptor to ON-bipolar synaptic transmission, the rectification in the postsynaptic membrane potential (which limits the bipolar cells' physiological response range to below -20 mV, thus seemingly marginalizing the band-pass filtering behavior) is actually a manifestation of the intrinsic dynamics of the bipolar cells and the action of potassium channels.

The activation of the potassium current may primarily produce an attenuation of gain to increase response speed, especially for the ON signals. Undershoots, associated with these changes, are an unmistakable signature (but not a necessary manifestation) of its activation. The kinetics of the potassium channel influence the detailed temporal features (including the undershoot) of the impulse response (Mao, 1996). Even in cases where the undershoot was not a strong feature, the general characteristics in gain and response speed persist. Near resting potential, gain as a function of mean current, has a peak that is so sharp that a current of a few pA would shift the operating point to a range with much reduced gain. Indeed, Tian and Slaughter (1995), from recordings of ON-bipolar cells of the salamander retinal slices, calculated that 45 synaptic channels are enough to substantially reduce gain and move membrane potential to a more depolarized level. It is thus unlikely that, in physiologic situations, a bipolar cell would consistently operate under high gain characteristics, specifically because of the nonlin-

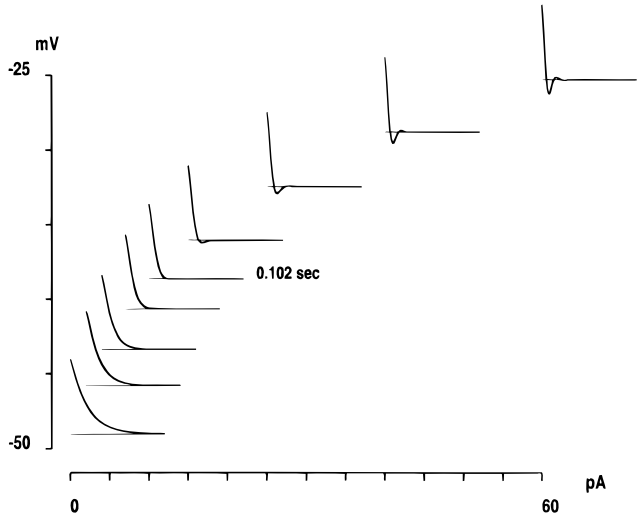

Fig. 11. Simulation: adaptive filter properties reconstructed. Impulse responses (estimated from literal impulses) for several mean currents are calculated for the model neuron (Table 1). Simulation results are presented in the same format as Fig. 5. The slope of static *V–I* curve is the sharpest near resting potential, and shallower for more depolarizing currents. Impulse responses are slow near resting potential. With depolarization, impulse responses become faster and have undershoots. At $t = 0$, all the impulse responses have a value of 0.1 $\mathrm{mV \cdot pA^{-1} \cdot ms^{-1}}$, consistent with the assumed capacitance of 10 pF. This is also consistent with our method of estimating capacitance by the reciprocal of the amplitude of impulse response at $t = 0$.

ear adaptive behavior we have demonstrated. In our preparation, some conductances might be lost in the isolated cells. If a substantial portion of the lost conductance are potassium channels, then in the intact retina, potassium currents might play an even larger role than in the isolated bipolar cells. Of note, bipolar cells in mice showed dense staining for potassium channels on dendrites and axon terminals, indicating possible functional roles for potassium channels in these regions (Klumpp et al., 1995).

Possible roles for the observed adaptive behavior

Synaptic and nonsynaptic conductances combine to set the synaptic gain from photoreceptor to bipolar cells. A match between the two is conducive to a high gain in dogfish (Ashmore & Falk, 1980; Falk, 1988). In toad retina, the ratio of the two conductances was estimated at 0.5 to 1.7 for hyperpolarizing bipolar cells (Belgum & Copenhagen, 1988). The high intrinsic gain of bipolar cells, which we observed, may be a postsynaptic requisite for achieving a high synaptic gain. On the other hand, the sharp decline of gain and time constant with small input currents may serve as a mechanism to regulate the gain and speed of response by the input. Without these adaptive changes, the bipolar cell would saturate if inputs are large or if inputs are small but sustained. Another possible role for the adaptive behavior may be related to the convergence of different signals, such as from rods and cones. The intrinsic adaptive behavior might allow one bipolar cell to operate in both dark and light states, conditions which require very different intrinsic gains. It is possible that the relative weight of intrinsic and synaptic conductances differs under different states of adaptation, and that with increasing light adaptation, the intrinsic conductance plays an increasingly important role in determining the dynamics of the bipolar cells.

Voltage-gated potassium conductances act to enhance and broaden frequency response of a bipolar cell. Nevertheless, the transfer functions at high frequencies, even with depolarization, are almost the same as the transfer function at the resting potential (Figs. 7A and 7B). High-frequency signals are thus transmitted in a fully linear fashion, independent of any slow signals upon which they are superimposed. This phenomenon bears fascinating similarity to what has been found during light adaptation in human psychophysics (Kelly, 1972), in turtle horizontal cells (Tranchina et al., 1984), and in the primate retinal ganglion cells (Purpura et al., 1990).

The above formal similarities, however, do not lead to the simple conclusion that bipolar cells' behavior accounts for light adaptation, since adaptation begins in individual rods and cones (Nakatani & Yau, 1988). Indeed, for any given light adaptation level, the intensity–response curve of bipolar cells has a steeper slope, thus narrower intensity range, than those of photoreceptors and horizontal cells (Werblin, 1971). Our results of a very high gain and a sharp gain drop upon small input currents are consistent with the narrow light intensity range of bipolar cells' light response curve. Psychophysical studies (Adelson, 1982) reveal two components in the time course of light adaptation: one is slow, which might correspond to the resetting of the operating curve *via* retinal networks; the other is nearly instantaneous, which might correspond to the intrinsic adaptation. The intrinsic dynamics we described may contribute to the fast phase of light adaptation.

Acknowledgments

This investigation was supported by NIH Grant EY9314. We thank Drs. Keith Purpura and Arlene Hirano for their helpful discussions, and Dr. Malcolm Slaughter for his suggestions.

References

Adelson, E.H. (1982). Saturation and adaptation in the rod system. *Vision Research* **22**, 1299–1312.

Armstrong, C.M., Swenson, R.P. & Taylor, S.R. (1982). Blocking of squid axon K channels by internal and external applied barium ions. *Journal of General Physiology* **80**, 663–682.

Ashmore, J.F. & Copenhagen, D.R. (1980). Different postsynaptic events in two types of retinal bipolar cells. *Nature* **288**, 84–86.

Ashmore, J.F. & Falk, G. (1979). Transmission of visual signals to bipolar cells near absolute threshold. *Vision Research* **19**, 419–423.

Ashmore, J.F. & Falk, G. (1980). Responses of rod bipolar cells in the dark-adapted retina of the dogfish, *Scyliorhinus canicula*. *Journal of Physiology* (London) **300**, 115–150.

Attwell, D. (1986). Ion channels and signal processing in the outer retina. *Quarterly Journal of Experimental Biology* **71**, 497–536.

Attwell, D., Borges, S., Wu, S.M. & Wilson, M. (1987). Signal clipping by the rod output synapse. *Nature* **328**, 522–524.

Bader, C.R., Bertrand, D. & Schwartz, E.A. (1982). Voltage-activated and calcium-activated currents studied in solitary rod inner segments from the salamander retina. *Journal of Physiology* (London) **331**, 253–284.

Baylor, D.A. & Hodgkin, A.L. (1974). Changes in time scale and sensitivity in turtle photoreceptors. *Journal of Physiology* (London) **242**, 729–758.

Belgum, J.H. & Copenhagen, D.R. (1988). Synaptic transfer of rod signals to horizontal and bipolar cells in the retina of the toad (*Bufo marinus*). *Journal of Physiology* (London) **396**, 225–245.

Capovilla, M., Hare, W.A. & Owen, W.G. (1987). Voltage gain of signal transfer from retinal rods to bipolar cells in the tiger salamander. *Journal of Physiology* (London) **391**, 125–140.

Copenhagen, D.R., Ashmore, J.F. & Schnapf, J.K. (1983). Kinetics of

synaptic transmission from photoreceptors to horizontal and bipolar cells in turtle retina. *Vision Research* **23**, 363–369.

ENROTH-CUGELL, C. & SHAPLEY, R.M. (1973). Adaptation and dynamics of cat retinal ganglion cells. *Journal of Physiology* (London) **233**, 271–309.

FALK, G. (1988). Signal transmission from rods to bipolar and horizontal cells: A synthesis. *Progress in Retinal Research* **8**, 255–279.

HARE, W.A., LOWE, J.S. & OWEN, G. (1986). Morphology of physiologically identified bipolar cells in the retina of the tiger salamander, *Ambystoma tigrinum*. *Journal of Comparative Neurology* **252**, 130–138.

HART, W.M. (1987). The temporal responsiveness of vision. In *Adler's Physiology of the Eye: Clinical Application*, ed. MOSES, R.A. & HART, W.M. pp. 429–457. St. Louis, Missouri: The C.V. Mosby Company.

HIRANO, A.A. & MACLEISH, P.R. (1991). Glutamate and 2-amino-4-phosphonobutyrate evoke an increase in potassium conductance in retinal bipolar cells. *Proceedings of the National Academy of Sciences of the U.S.A.* **88**, 805–809.

HODGKIN, A.L. & HUXLEY, A.F. (1952). A quantitative description of membrane current and its application to conductance and excitation in nerve. *Journal of Physiology* (London) **117**, 500–544.

KANEKO, A. & TACHIBANA, M. (1981). Retinal bipolar cells with double color-opponent receptive fields. *Nature* **293**, 220–222.

KANEKO, A. & TACHIBANA, M. (1985). A voltage-clamp analysis of membrane currents in solitary bipolar cells dissociated from *Carassius auratus*. *Journal of Physiology* (London) **358**, 131–152.

KANEKO, A. & TACHIBANA, M. (1986). Membrane properties of solitary retinal cells. *Progress in Retinal Research* **5**, 125–146.

KARSCHIN, A. & WÄSSLE, H. (1990). Voltage- and transmitter-gated currents in isolated rod bipolar cells of rat retina. *Journal of Neurophysiology* **63**, 860–876.

KELLY, D.H. (1972). Adaptation effects on spatio-temporal sine-wave thresholds. *Vision Research* **12**, 89–101.

KIM, H.G. & MILLER, R.F. (1993). Properties of synaptic transmission from photoreceptors to bipolar cells in the mudpuppy retina. *Journal of Neurophysiology* **69**, 352–360.

KLUMPP, D.J., SONG, E.J., ITO, S., SHENG, M.H., JAN, L.Y. & PINTO, L.H. (1995). The shaker-like potassium channels of the mouse rod bipolar cell and their contributions to the membrane current. *Journal of Neuroscience* **15**, 5004–5013.

LASANSKY, A. (1992). Properties of depolarizing bipolar cell responses to central illumination in salamander slices. *Brain Research* **576**, 181–196.

LASATER, E.M., DOWLING, J.E. & RIPPS, H. (1984). Pharmacological properties of isolated horizontal and bipolar cells from the skate retina. *Journal of Neuroscience* **4**, 1966–1975.

LASATER, E.M. (1988). Membrane currents of retinal bipolar cells in culture. *Journal of Neurophysiology* **60**, 1460–1480.

MACLEISH, P.R., BARNSTABLE, C.J. & TOWNES-ANDERSON, E. (1983). Use of monoclonal antibody as a substrate for mature neurons *in vitro*. *Proceedings of the National Academy of Sciences of the U.S.A.* **80**, 7014–7018.

MACLEISH, P.R., SCHWARTZ, E.A. & TACHIBANA, M. (1984). Control of the generator current in solitary rods of the *Ambystoma tigrinum* retina. *Journal of Physiology* (London) **348**, 645–664.

MAO, B. (1996). *The intrinsic dynamics of retinal bipolar cells and their ion channel mechanisms*. Ph.D. Thesis, Cornell University.

MAO, B., MACLEISH, P.R. & VICTOR, J.D. (1995). Dynamics of isolated retinal bipolar cells in the tiger salamander. *Society for Neuroscience Abstracts* **21**, 389.

MAO, B., MACLEISH, P.R. & VICTOR, J.D. (1996). Voltage-dependent potassium current is sufficient for the changes in gain and dynamics of isolated retinal bipolar cells of the tiger salamander. *Investigative Ophthalmology and Visual Science* **37**, S1054.

MARMARELIS, P.Z. & MARMARELIS, V.Z. (1978). *Analysis of Physiological Systems: The White Noise Approach*. New York: Plenum Press.

NAKA, K-I, MARMARELIS, P.Z. & CHAN, R.Y. (1975). Morphological and functional identifications of catfish retinal neurons. III. Functional identification. *Journal of Neurophysiology* **38**, 92–138.

NAKATANI, K. & YAU, K.-W. (1988). Calcium and light adaptation in retinal rods and cones. *Nature* **334**, 69–71.

NAWY, S. & JAHR, C.E. (1990). Suppression by glutamate of cGMP-activated conductance in retinal bipolar cells. *Nature* **346**, 269–271.

PRESS, W.H., TEUKOLSKY, S.A., VETTERLING, W.T., & FLANNERY, B.P. (1992). *Numerical Recipes in C* (2nd edition). New York: Cambridge University Press.

PURPURA, K., TRANCHINA, D., KAPLAN, E. & SHAPLEY, R.M. (1990). Light adaptation in the primate retina: Analysis of changes in gain and dynamics of monkey retinal ganglion cells. *Visual Neuroscience* **4**, 75–93.

RUDY, B. (1988). Diversity and ubiquity of K channels. *Neuroscience* **25**, 729–749.

SHIELLS, R.A. & FALK, G. (1992). Properties of the cGMP-activated channel of retinal on-bipolar cells. *Proceedings of the Royal Society B* (London) **247**, 21–25.

SHIELLS, R.A., FALK, G. & NAGHSHINEH, S. (1981). Action of glutamate and aspartate analogues on rod horizontal and bipolar Cells. *Nature* **294**, 592–594.

SLAUGHTER, M.M. & MILLER, R.F. (1981). 2-amino-4-phosphonobutyric acid: A new pharmacological tool for retina research. *Science* **211**, 182–185.

SUTTER, E.E. (1987). A practical nonstochastic approach to nonlinear time-domain analysis. In *Advanced Methods in Physiological System Modelling. Vol. 1*, ed. MARMARELIS, V.Z., pp. 303–315. Los Angeles, California: University of Southern California.

TESSIER-LAVIGNE, M., ATTWELL, D., MOBBS, P. & WILSON, M. (1988). Membrane currents in retinal bipolar cells of the axolotl. *Journal of General Physiology* **91**, 49–72.

TIAN, N. & SLAUGHTER, M.M. (1995). Functional properties of a metabotropic glutamate receptor at dendritic synapses of on-bipolar cells in the amphibian retina. *Visual Neuroscience* **12**, 755–765.

TRANCHINA, D., GORDON, J. & SHAPLEY, R. (1984). Retinal light adaptation—evidence for a feedback mechanism. *Nature* **310**, 314–331.

VICTOR, J.D. (1988). The dynamics of the cat retinal Y-cell subunit. *Journal of Physiology* (London) **405**, 289–320.

VICTOR, J.D. (1992). Nonlinear system analysis in vision: Overview of kernel methods. In *Nonlinear Vision*, ed. PINTER, R.B. & NABET, B., pp. 1–37. Boca Raton, Florida: CRC Press.

WERBLIN, F.S. (1971). Adaptation in a vertebrate retina: Intracellular recording in *necturus*. *Journal of Neurophysiology* **34**, 228–241.

WERBLIN, F.S. & DOWLING, J.E. (1969). Organization of the retina of mudpuppy *Necturus maculosus*. II. Intracellular recording. *Journal of Neurophysiology* **32**, 339–355.

WU, S.M. (1991). Signal transmission and adaptation-induced modulation of photoreceptor synapses in the retina. *Progress in Retinal Research* **10**, 27–44.

WU, S.M. & YANG, X.-L. (1992). Modulation of synaptic gain by light. *Proceedings of the National Academy of Sciences of the U.S.A.* **89**, 11755–11758.